Advanced Energy Materials

ADVANCED ENERGY MATERIALS
www.advenergymat.de

RESEARCH ARTICLE OPEN ACCESS

Pt Single-Atom Catalysts on FTO for Optically Invisible pH-Universal Hydrogen Evolution Electrodes

Jihyeon Kim[1] | Xin Zhou[1] | Dmitry E. Doronkinb[2] | Bidyut Bikash Sarmac[3] | Ana S. Dobrota[4] | Natalia V. Skorodumova[5] | Igor A. Pašti[4,6] | Jochen Schmidt[7] | Patrik Schmuki[1,8]

[1]Department of Materials Science and Engineering, Chair for Surface Science and Corrosion (WW4-LKO), Friedrich-Alexander-Universität Erlangen-Nürnberg, Erlangen, Germany | [2]Institute For Chemical Technology and Polymer Chemistry and Institute of Catalysis Research and Technology, Karlsruhe Institute of Technology, Karlsruhe, Germany | [3]LCC: Laboratoire de Chimie de Coordination, (LCC), CNRS, Universite de Toulouse, INPT, Toulouse, France | [4]University of Belgrade – Faculty of Physical Chemistry, Belgrade, Serbia | [5]Applied Physics, Division of Materials Science, Department of Engineering Sciences and Mathematics, Luleå University of Technology, Luleå, Sweden | [6]Serbian Academy of Sciences and Arts, Belgrade, Serbia | [7]Institute of Interfaces and Particle Technology (IPT), Erlangen, Germany | [8]Regional Centre of Advanced Technologies and Materials, Czech Advanced Technology and Research Institute (CATRIN), Palacký University, Olomouc, Czech Republic

Correspondence: Patrik Schmuki (schmuki@ww.uni-erlangen.de)

Received: 6 February 2026 | **Revised:** 20 July 2026 | **Accepted:** 30 July 2026

Keywords: catalysis | electrode | electrochemistry | Hydrogen | Pt single atom | tin oxide

ABSTRACT

Transparent hydrogen-evolution electrodes are essential for photoelectrochemical and optoelectronic energy-conversion devices, yet typically suffer from a trade-off between catalytic activity and optical transmission. Here, we demonstrate that an ultra-low loading of Pt single atoms (SA, 0.03 at%) directly anchored on fluorine-doped tin oxide (FTO) via a reactive deposition delivers hydrogen evolution reaction (HER) kinetics approaching bulk Pt, while remaining optically invisible. At this low SA loading, HAADF-STEM directly resolves atomically isolated Pt sites, while x-ray photoelectron and absorption spectroscopy confirm exclusively cationic $Pt^{\delta+}$ ($\delta \approx 2$) in Pt–O_4 coordination. The Pt SA/FTO electrodes exhibit pH-universal HER activity, alongside turnover frequencies exceeding 500 s^{-1} at moderate overpotentials. Density Functional Theory calculations support the high stability of Pt SA/FTO and explain exceptional HER activity by optimized energetics of intermediate formation. Achieving comparable kinetics with conventional sputtered Pt films requires >1000-fold higher Pt loading and leads to substantial optical losses. Owing to its optical neutrality, the Pt SA/FTO electrode enables 2–3 × higher photocurrents than activity-matched Pt films when used as a counter electrode in sandwich-type photoelectrochemical cells. These results on Pt SA-decorated FTO thus describe a general strategy to unite noble-metal utilization, high catalytic efficiency, and optical transparency in electro- and photoelectrochemical devices.

1 | Introduction

Transparent conductive oxides such as fluorine-doped tin oxide (FTO) are essential components in photoelectrochemical (PEC) architectures, spectroelectrochemical platforms, and operando optical studies, due to the combination of optical transparency, chemical robustness, and electrical conductivity [1–5]. In water-splitting and related energy-conversion devices, FTO is frequently employed as a counter electrode or current collector positioned directly in the optical path, where minimizing absorption losses is essential for efficient device operation. However, activating such transparent electrodes for efficient hydrogen evolution (HER) typically requires the introduction of noble-metal catalysts, most commonly Pt, which inevitably

introduces a trade-off between catalytic activity and optical transmission.

To provide HER activity, FTO surfaces are conventionally decorated with Pt using a variety of established approaches, including thermal platinization of Pt precursors, atomic layer deposition, electrodeposition or electrophoretic deposition, chemical wet reduction, UV-assisted photoreduction, and sputter- or evaporation-based thin-film deposition, often followed by thermal annealing [6–14]. While these methods can provide high catalytic activity, they consistently result in the formation of Pt nanoparticles, clusters, or continuous ultrathin films. Moreover, achieving reasonable HER kinetics generally requires relatively high Pt loadings, which affect optical transparency and lead to inefficient noble-metal utilization. Even strategies such as solid-state dewetting of ultrathin Pt films — while improving transparency and metal–support interactions—still rely on nanoscale Pt ensembles rather than atomically dispersed sites and therefore do not fully overcome this fundamental activity–transparency trade-off [7]. Resolving this trade-off therefore requires a catalyst configuration that decouples HER activity from optical absorption — a condition that nanoparticulate or film-based Pt cannot fulfill in principle.

In this context, using Pt as dispersed single atoms (SAs) offers an extreme atom economy by exposing every metal atom as an accessible site, while support interactions may strongly alter catalytic reaction barriers [15, 16]. Accordingly, Pt single-atom catalysts have demonstrated exceptionally high mass activities for hydrogen evolution and related reactions, particularly on carbon-based supports and photocatalytic oxide substrates [16–18]. However, despite these advances, the direct implementation of Pt single atoms on transparent, conductive oxides has remained largely unexplored. This is particularly surprising when considering the potential for a unique combination of low loading/high activity and concomitant minimization of optical transparency losses.

FTO represents a particularly attractive platform for stabilizing Pt single atoms while enabling efficient electrocatalysis. Besides its macroscopic conductivity, Pt–SnO_2 interfaces are known to exhibit distinct electronic metal–support interaction (EMSI) effects that can enhance hydrogen evolution kinetics [1, 7, 19]. At the atomic scale, the SnO_2 lattice provides oxygen-coordinated cationic sites and oxygen-vacancy motifs capable of stabilizing cationic Pt species ($Pt^{\delta+}$) through strong Pt–O(Sn) coordination [20]. Such stabilization is especially relevant for hydrogen evolution in neutral and alkaline media, where water activation becomes kinetically demanding and oxide-assisted pathways can lower the effective Volmer barrier. These considerations suggest that conductive oxides such as FTO can function not only as current collectors, but as chemically and electronically active hosts for single-atom catalytic sites.

Here, we report a room-temperature reactive deposition strategy that enables the direct anchoring of isolated Pt single atoms on fluorine-doped tin oxide without applied bias or illumination. This approach yields a sub-monolayer population of atomically dispersed Pt sites at an ultralow total loading of only 0.03 at%, while fully preserving the optical transparency of the FTO substrate. Despite the extremely low Pt density, the resulting Pt single-atom/FTO electrodes exhibit hydrogen evolution reaction kinetics approaching those of bulk Pt across acidic, neutral, and alkaline electrolytes.

2 | Results and Discussion

To deposit Pt single atoms by reactive deposition, we followed an approach previously established for other oxide substrates, which relies on a surface displacement reaction between H_2PtCl_6 and redox-active sites on the oxide surface [18, 21, 22]. For this, commercial FTO substrates were exposed to a dilute chloroplatinic acid solution (10 mM H_2PtCl_6) for 1 h under ambient conditions (see Supporting Information for details). After treatment, no macroscopic modification of the FTO surface is observed: optical images and high-resolution SEM (Figure 1a and Figure S1) show neither surface etching nor the formation of Pt nanoparticles or agglomerates ≥1 nm (resolution limit of HR-SEM).

In contrast, high-angle annular dark-field scanning transmission electron microscopy (HAADF-STEM) shows the successful deposition of atomically isolated Pt species on the FTO surface (Figure 1b, Pt SAs marked with yellow circles). The underlying lattice spacings of 0.13, 0.16, and 0.26 nm can be indexed to the (310), (211), and (101) planes of SnO_2, respectively, in agreement with the XRD pattern of the FTO substrate (Figure S2) [23, 24]. Importantly, the Pt SAs are uniformly dispersed across the surface, yielding an areal density of $\approx 2.7 \times 10^5$ μm^{-2} as determined by direct atom counting from multiple STEM images. Energy-dispersive x-ray spectroscopy (EDXS) mapping further confirms the homogeneous Pt distribution and the absence of Pt agglomerates (Figure 1c).

High-resolution x-ray photoelectron spectroscopy (XPS) of the Pt 4f region exhibits a single doublet with Pt $4f_{7/2}$ and Pt $4f_{5/2}$ peaks at 72.8 and 76.2 eV, respectively (Figure 1d and Figure S3), characteristic of cationic $Pt^{\delta+}$ species with $\delta \approx 2$. No contribution from metallic Pt^0 is detected. To further investigate the local coordination environment of Pt SAs on FTO, x-ray absorption spectroscopy (XAS) was performed at the Pt L_3-edge. Since direct XAS analysis of the planar FTO electrodes was not feasible due to the extremely low Pt loading, FTO powder decorated with Pt SAs by the same reactive deposition procedure was used instead. Prior to the XAS measurements, we verified that the characteristic Pt SA features were preserved on the powder substrate. As shown in Figure 2a, the Pt 4f XPS spectrum of Pt SA on FTO powder shows a Pt $4f_{7/2}$ and $4f_{5/2}$ doublet at 72.9 and 76.2 eV, respectively, consistent with $Pt^{\delta+}$ ($\delta \approx 2$) as observed for the FTO film (Figure 1d), and the powder-supported sample exhibits nearly identical HER behavior and Tafel slope (Figure 2b). The x-ray absorption near-edge structure (XANES) spectrum of Pt SA on FTO powder (Figure 2c) shows a white-line intensity intermediate between those of the Pt foil and PtO_2 references, indicating a partially oxidized Pt species, in agreement with the XPS results. The corresponding Fourier transform of the extended x-ray absorption fine structure (FT-EXAFS, Figure 2d) spectrum is dominated by a single first-shell feature at an apparent radial distance of ≈1.65 Å (phase-uncorrected), assigned to Pt–O coordination. Quantitative fitting of the first shell yields a Pt–O coordination number of 4.0 ± 0.4 at a phase-corrected distance of $R = 2.02$ Å (Figure S4). The combination of the Pt 4f

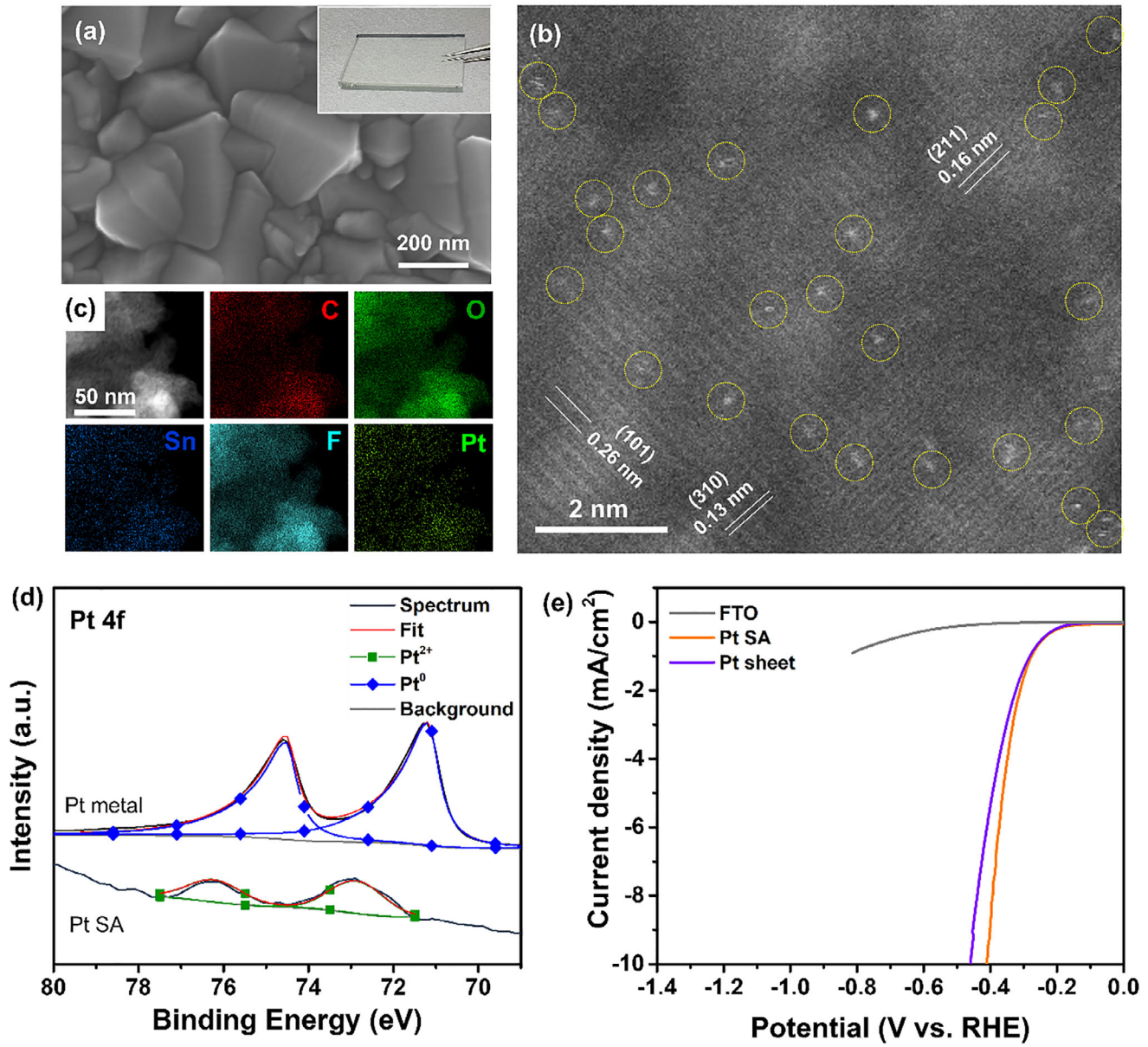

FIGURE 1 | (a) SEM image (inset: optical image), (b) HAADF-STEM image, and (c) the corresponding element mapping images of Pt SA on FTO. (d) XPS Pt 4f spectra and (e) LSV curves of bare FTO, Pt SA on FTO, and Pt sheet (0.1 M Na_2SO_4).

binding energy from XPS, the intermediate white-line intensity from XANES, and the fitted fourfold Pt–O coordination from EXAFS consistently indicates isolated Pt species with an average oxidation state close to +2 ($Pt^{\delta+}$, $\delta \approx 2$). Importantly, no Pt–Pt scattering contribution is detected at the position of the first-shell Pt–Pt peak of the Pt foil reference, ruling out the presence of Pt clusters or nanoparticles. The dominant Pt–O coordination together with the absence of Pt–Pt scattering is the established EXAFS signature of atomically dispersed, oxygen-coordinated Pt species on oxide supports [21, 22, 46], and is fully consistent with Pt^{2+} anchored on O(Sn) sites of the SnO_2 lattice, formed by ligand exchange between H_2PtCl_6 and oxygen-coordinated surface sites [20, 25] in line with the $Pt^{4+} \rightarrow Pt^{2+}$ reduction reported for reactive deposition on other oxide supports [18, 21, 22].

Quantitative evaluation of the Pt 4f XPS spectra yields an exceptionally low surface concentration of approximately 0.03 at% Pt. Converting this value into an areal single-atom density using standard XPS assumptions regarding the information depth and uniform surface distribution (see Figure S5) results in a density of 1–3 × 10^5 μm^{-2}. Notably, this range is in excellent agreement with the value independently obtained from direct HAADF-STEM atom counting (≈2.7 × 10^5 μm^{-2}), confirming that the STEM-observed density is representative of the entire electrode surface rather than a local high-loading region. As the XPS-based estimate assumes a homogeneous Pt distribution within the probing depth, this agreement further indicates that the derived site density is conservative.

Remarkably, despite this ultralow Pt loading, the Pt SA/FTO electrode exhibits a pronounced hydrogen evolution activity. Figure 1e compares linear sweep voltammetry (LSV) curves recorded in 0.1 M Na_2SO_4 for Pt SA/FTO, bare FTO, and a bulk Pt foil reference. The Pt SA/FTO electrode displays HER

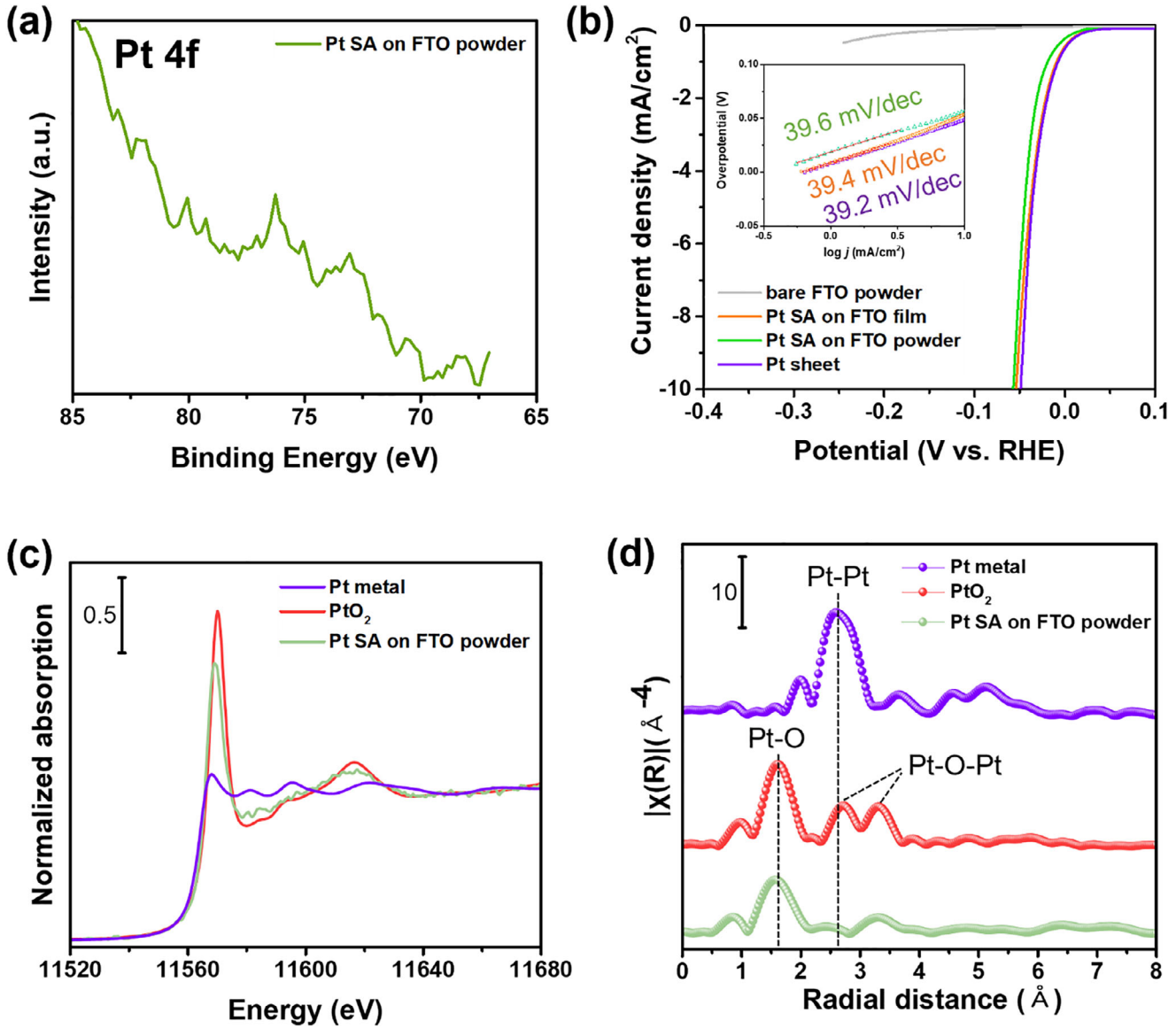

FIGURE 2 | (a) XPS Pt 4f spectra, (b) LSV curves in 0.1 M H_2SO_4 (inset shows corresponding Tafel slope) of Pt SA on FTO powder. (c) Pt L_3-edge normalized XANES spectra and (d) the corresponding FT-EXAFS spectra of Pt foil, PtO_2, and Pt SA on FTO powder.

characteristics closely matching those of Pt foil, while bare FTO remains essentially inactive. The observed activity in neutral electrolyte is fully consistent with literature reports on Pt-based HER electrocatalysts under comparable conditions [17, 26].

This high catalytic efficiency of the low-loading Pt SA/FTO electrode is not limited to neutral electrolytes but extends across acidic and alkaline pH values (Figure 3). In acidic solution (0.1 M H_2SO_4, Figure 3a), the Pt SA/FTO electrode exhibits a Tafel slope of 39.4 mV dec^{-1}, indistinguishable from that of Pt foil (39.2 mV dec^{-1}), consistent with the well-established high activity of Pt in the Heyrovský/Tafel regime. This behavior aligns with previous reports on Pt supported on F-doped 3-D SnO_2 nanostructures or high-activity dewetted structures, where strong electronic metal–support interaction (EMSI) effects were shown to accelerate HER kinetics [1, 7, 19]. For example, Lai et al., reported that the interfacial electron coupling at the Pt-SnO_2 interface downshifts the Pt d-band center and optimizes H* adsorption/desorption behavior, accounting for the enhanced HER kinetics of the Pt/SnO_2 system [19]. In particular, the Pt on F-doped SnO_2 system has been well described by DFT in the work of Kim et al., which demonstrated that orbital hybridization between Pt and F-SnO_2 enhances H* adsorption at the Pt–support interface, directly improving the HER kinetics [1].

Moreover, the Pt SA/FTO electrode shows excellent electrochemical stability under HER conditions. After 3000 CV cycles in 0.1 M H_2SO_4 (Figure S6), the polarization curve shows negligible degradation. To examine the structural stability of the Pt/FTO electrode after HER operation, post-HER SEM analysis was performed (Figure S7). The overall FTO surface morphology was largely retained, although a few Pt NPs were observed, indicating partial reduction of Pt species during HER. Notably, the polarization behavior is essentially identical from the initial cycle to after 3000 cycles, indicating that the minor restructuring does not contribute measurably to the observed activity and

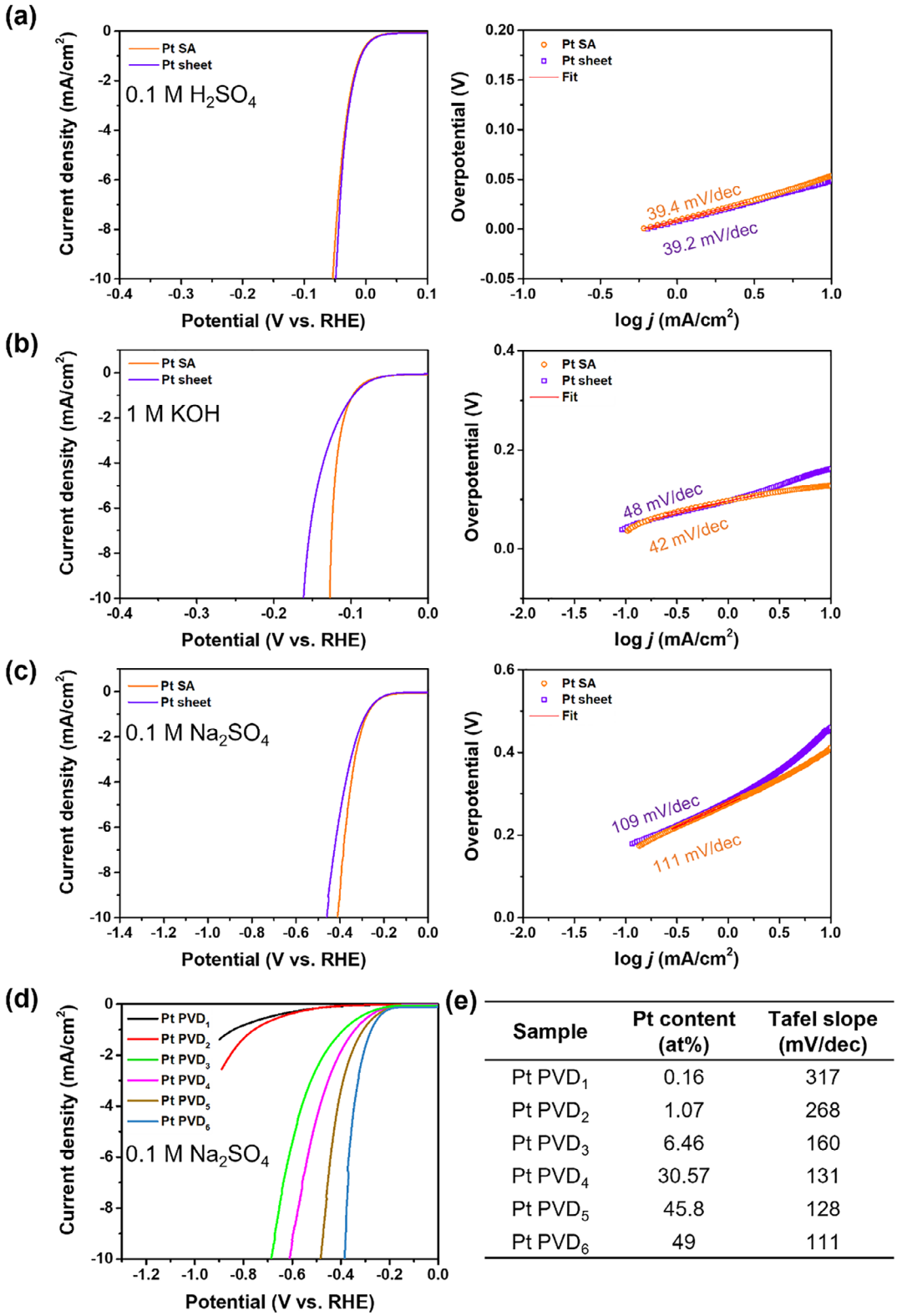

(e)

Sample	Pt content (at%)	Tafel slope (mV/dec)
$Pt\ PVD_1$	0.16	317
$Pt\ PVD_2$	1.07	268
$Pt\ PVD_3$	6.46	160
$Pt\ PVD_4$	30.57	131
$Pt\ PVD_5$	45.8	128
$Pt\ PVD_6$	49	111

FIGURE 3 | LSV curves and corresponding Tafel plots of Pt SA on FTO and Pt sheet in (a) 0.1 M H_2SO_4, (b) 1 M KOH, and (c) 0.1 M Na_2SO_4. (d) LSV curves taken in 0.1 M Na_2SO_4 and (e) data of Pt content and Tafel slope of Pt PVD electrodes.

that the dominant active-site population is established upon deposition.

Most notably, in alkaline electrolyte (1 M KOH, Figure 3b), Pt SA/FTO reaches a Tafel slope of 42 mV dec^{-1}, comparable to that of Pt foil (48 mV dec^{-1}), which is exceptionally low for atomically dispersed Pt on an oxide support [27–29]. Importantly, this alkaline activity cannot be attributed to pre-existing Pt clusters or nanoparticles, as HAADF-STEM, XPS, and XANES/EXAFS consistently show that the as-prepared electrodes contain exclusively

atomically dispersed $Pt^{\delta+}$ with no Pt–Pt contribution. Instead, the observed alkaline activity is consistent with facilitated water activation at $Pt^{\delta+}$–O(Sn) interfacial sites, placing Pt SA/FTO among the small number of single-atom systems that achieve bulk-like alkaline HER kinetics without the need for intentionally engineered bifunctional supports [30–32].

In neutral electrolyte (0.1 M Na_2SO_4, Figure 3c), the Tafel slope increases to 111 mV dec^{-1} for Pt SA/FTO and 109 mV dec^{-1} for Pt foil, consistent with Volmer-limited kinetics where water dissociation becomes rate-relevant. The close correspondence between Pt SA/FTO and bulk Pt again indicates that $Pt^{\delta+}$ sites electronically coupled to FTO do not introduce an additional kinetic hindrance in neutral media.

To compare the performance of the Pt SA/FTO electrodes to conventional Pt metallization, Pt was sputter-deposited onto identical FTO substrates with increasing loadings using a physical vapor deposition (PVD) approach following Ref. [33]. Figure 3d shows the corresponding LSV curves recorded in neutral electrolyte, while Figure 3e summarizes the Pt surface concentration derived from XPS together with the extracted Tafel slopes (Figure S8). With increasing Pt loading, the HER kinetics improve gradually and only approach bulk-Pt behavior at surface concentrations of approximately 40–50 at% Pt.

XPS analysis of these PVD-loaded samples reveals exclusively metallic Pt^0, while SEM images show the formation of nanoscale Pt clusters with characteristic sizes of ≈1 nm (Figure S9). Thus, to achieve neutral-pH HER kinetics comparable to those of the Pt SA/FTO electrode, conventional PVD deposition requires a Pt surface concentration that is more than three orders of magnitude higher in terms of accessible Pt surface atoms. This comparison underscores the markedly higher Pt utilization efficiency achieved by atomically dispersed Pt on FTO relative to nanoparticle- or film-based Pt electrodes.

The enhanced HER kinetics of Pt SA/FTO are further reflected in electrochemical impedance spectroscopy (EIS) measurements. Nyquist plots recorded in 0.1 M Na_2SO_4 and fitted using a classical Randles equivalent circuit are shown in Figure S10, with the extracted parameters summarized in Table S1. The Pt SA/FTO electrode exhibits a charge-transfer resistance (R_{ct}) of 102.2 Ω cm^2, which is substantially lower than that of bare FTO (4887.1 Ω cm^2) and approaches the value observed for a highly loaded PVD-Pt electrode (Pt PVD_6, 27.5 Ω cm^2).

In contrast, the low-loading PVD-Pt electrode (Pt PVD_1), which contains a similar overall Pt amount as the Pt SA/FTO sample, displays an R_{ct} value (3052.9 Ω cm^2) comparable to that of native FTO. These results are consistent with the LSV and Tafel analyses and indicate that atomically dispersed Pt on FTO enables efficient interfacial charge transfer at ultralow Pt loadings, whereas nanoscale Pt ensembles only become effective at substantially higher surface coverage.

To further quantify the intrinsic activity of the Pt SA/FTO electrodes, turnover frequencies (TOFs) were estimated using the experimentally determined single-atom density of 1–3 × 10^5 μm^{-2} derived from STEM and XPS analyses. Based on the measured

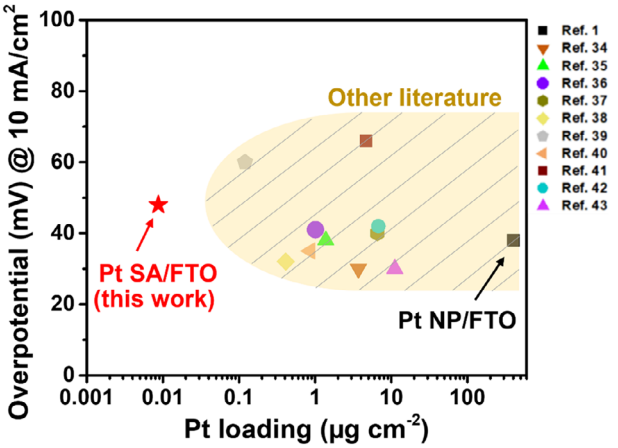

FIGURE 4 | Comparison of the overpotential (η) at 10 mA cm^{-2} in acidic electrolyte of Pt SA on FTO (this work) and other literature.

geometric current densities and assuming unity Faradaic efficiency for hydrogen evolution (as is standard for Pt-based HER catalysts), TOFs of 260–770 s^{-1} in acidic media (at η = 25 mV), 120–350 s^{-1} in alkaline media (at η = 100 mV), and 140–430 s^{-1} in neutral media (at η = 300 mV) are obtained (Table S2). Notably, TOFs on the order of 500 s^{-1} are reached at relatively modest overpotentials of 20–40 mV (acidic), 110–120 mV (alkaline), and 300–360 mV (neutral). To further benchmark the catalytic efficiency of the Pt SA/FTO electrode, we compared the Pt loading and overpotential required to reach 10 mA cm^{-2} (η_{10}) with previously reported Pt SA- and NP-based HER catalysts (Figure 4) [1, 27, 34–42]. The Pt SA/FTO electrode exhibits a very low Pt loading (≈2.7 × 10^5 μm^{-2}), while maintaining a competitive HER overpotential (η_{10}). In particular, a previously reported Pt NP/FTO catalyst [1] reaches a comparable overpotential but requires an orders-of-magnitude higher Pt loading. These results place Pt SA/FTO among the most active Pt single-atom HER catalysts reported to date [43], highlighting the exceptional utilization efficiency of atomically dispersed Pt on a conductive oxide support.

To explain the high HER activity of the Pt SA/FTO electrode, we have performed DFT calculations on model Pt SAs and a Pt_4 cluster on the FTO surface, comparing the energetics of adsorbed H (H_{ads}) formation with that on the Pt(111) surface. We note that the simulated XRD patterns of FTO, compared with those of the optimized SnO_2 (Figure S11), agree well with the experimental ones (Figure S2), indicating a slight expansion of the lattice with F doping. The most stable structure of Pt SA on FTO (Figure 5a) provides ΔG_H of only 0.02 eV, which is better optimized for superb HER activity than Pt(111), with ΔG_H between −0.08 and −0.03 eV, depending on the coverage [44]. In this configuration, Pt SA has a Bader charge of +1.35 e, somewhat less than the formal +2 charge. The optimized Pt SA model displays a distorted fourfold Pt–O coordination environment, with an average Pt–O bond length of 1.9 Å. This coordination motif is consistent with the FT-EXAFS analysis (Figure 2d and Figure S4), which indicates a Pt–O first shell with a fitted average distance of 2.02 Å. The difference between the calculated and experimental distances is reasonable considering the distorted surface coordination of the Pt single atom, the distribution of local environments expected in the real material, the fact that

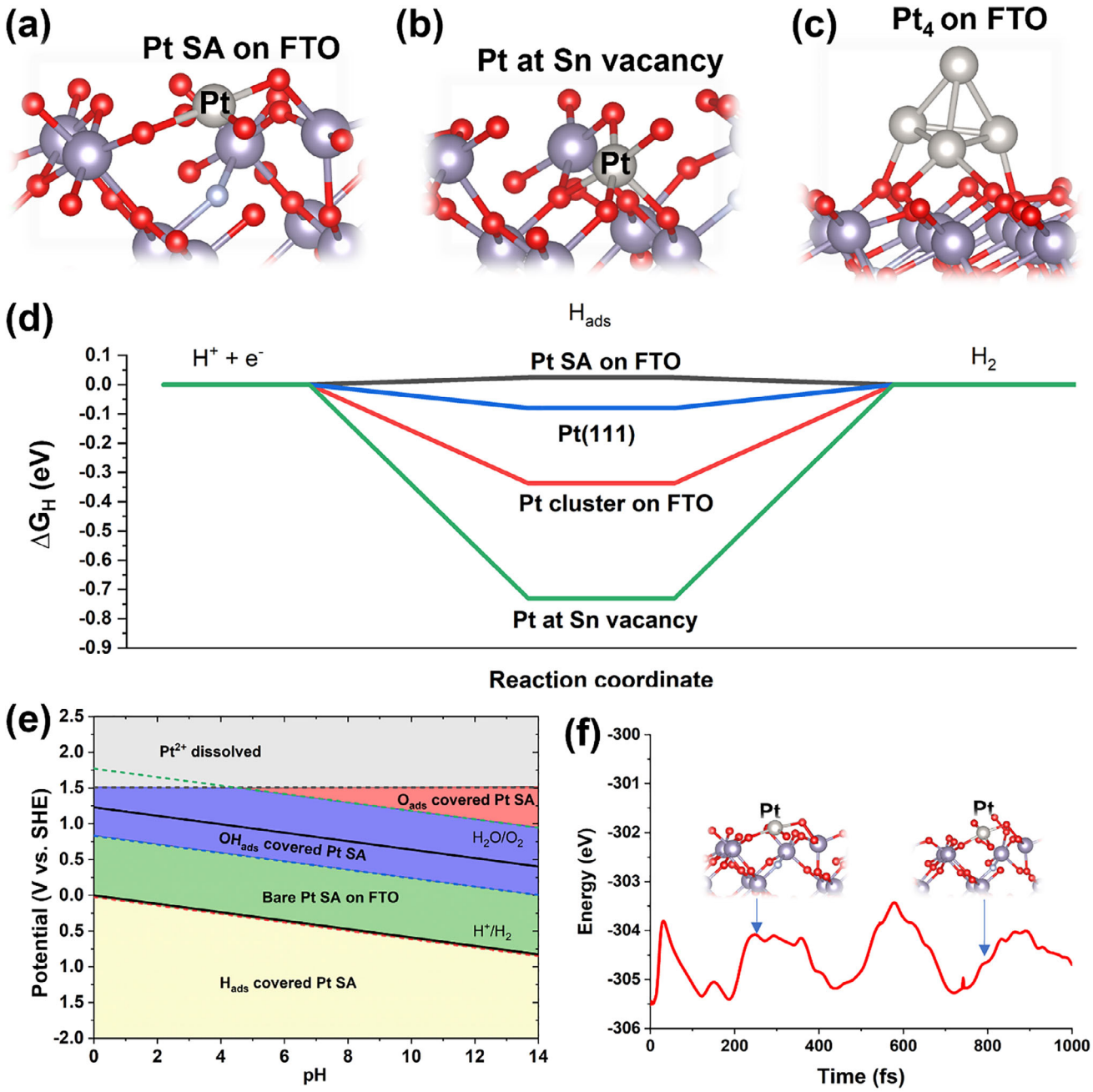

FIGURE 5 | Theoretical modelling of Pt on FTO. Top row: DFT optimized structures of (a) Pt SA adsorbed onto FTO, (b) Pt SA embedded into Sn-vacancy in FTO, (c) Pt_4 cluster on FTO. Middle row: (d) HER reaction profile on the studied Pt-on-FTO models, with Pt(111) added as a reference. Bottom row: (e) Pourbaix diagram of Pt SA/FTO; (f) Time evolution of the Pt SA/FTO at 300 K (from ab initio molecular dynamics) showing that the system is kinetically stable, insets give structure snapshots during the simulation.

FT-EXAFS provides an averaged first-shell structural parameter, and the applied level of theory. Notably, both experiment and theory support the same structural picture of an isolated cationic Pt center coordinated to lattice oxygen atoms, rather than metallic Pt aggregates. In contrast, Pt SA, which substitutes Sn (Figure 5b), binds H_{ads} much more strongly ($\Delta G_H = -0.73$ eV). Despite also having a Bader charge of +1.35 e, this model is a five-coordinated Pt SA, indicating that this local structure is not the experimentally observed one. To model the PVD electrode, we placed a Pt_4 cluster on the FTO surface (Figure 5c). In this cluster, Pt atoms remain nearly metallic (average Bader charge of Pt +0.25 e), while H binds strongly to it, with ΔG_H of −0.34 eV. By constructing the HER reaction profile (Figure 5d) according to [44] one can see that the order of HER activity should be {Pt SA/FTO} ≥ {metallic Pt} > {Pt subnanoclusters on FTO}, suggesting that the activity is maximized by Pt SA deposition on the FTO surface, where the improved H_{ads} formation energetics compensates the lower active site density compared to bulk Pt surface. As ΔG_H can be considered a universal descriptor of HER activity [45], the optimized H_{ads} energetics on Pt SA/FTO justify high HER activity irrespective of the electrolyte pH.

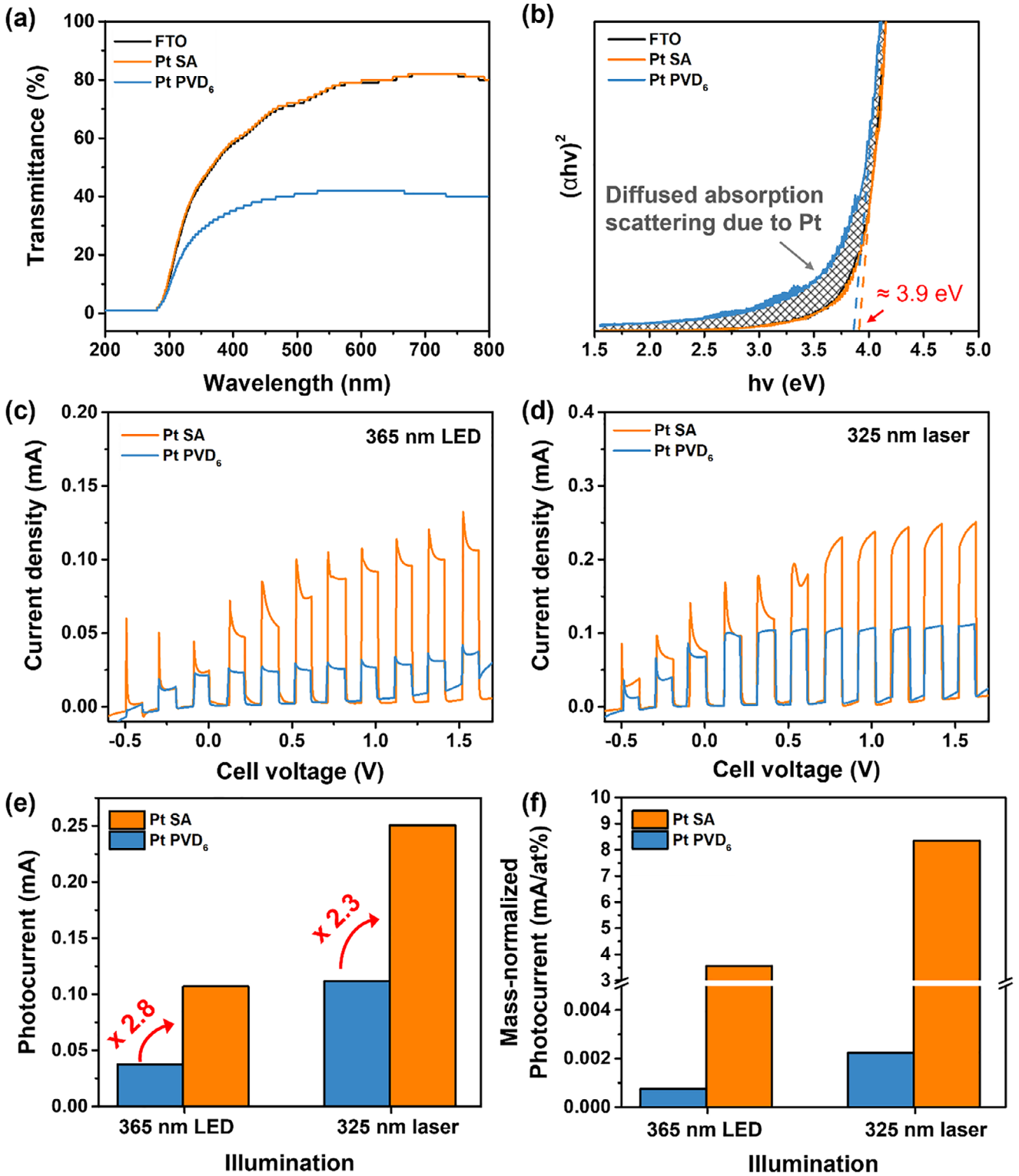

FIGURE 6 | (a) Transmittance and (b) Tauc plot of bare FTO, Pt SA, and Pt PVD_6. LSV curves for photoelectrochemical water splitting of the TiO_2 layer using Pt SA and Pt PVD_6 as a counter electrode under front illumination with (c) 365 nm LED and (d) 325 nm laser. (e) Photocurrent and (f) mass-normalized photocurrent density at 1.6 V of the TiO_2 layer using Pt SA and Pt PVD_6 as a counter electrode under front illumination (365 nm LED and 325 nm laser).

To examine the state of the Pt SA/FTO under electrochemical conditions, we constructed a Pourbaix plot for this system (Figure 5e). Strong binding of Pt on the FTO surface (−6.99 eV), surpassing the cohesive energy of Pt, stabilizes Pt SAs against dissolution. Furthermore, Pt SAs do not exhibit increased oxophilicity compared to metallic Pt, and the deposition of O and OH starts at high anodic potentials. Thus, at potentials just before the HER onset, the Pt SA/FTO is bare and "HER-ready", free from spectating oxygen species. Strong Pt SA binding also leads to the conclusion that Pt aggregation is not likely, but this was explicitly checked using ab initio molecular dynamics at 300 K (Figure 5f). The results show that the Pt SA/FTO structure is stable over time and that the Pt atom retains its coordination, which warrants high HER activity.

Beyond catalytic efficiency, the ultralow Pt loading provides a decisive advantage in terms of optical transparency. Figure 6a shows the total transmittance spectra $T(\lambda)$ of bare FTO and Pt SA/FTO electrodes, which are essentially indistinguishable across the visible and near-infrared range, confirming the optical neutrality of the atomically dispersed Pt layer. No plasmonic features or measurable increase in absorption are observed, consistent with the absence of metallic Pt nanoparticles [46, 47].

The corresponding Tauc plots (Figure 6b) reveal identical optical band gaps of approximately 3.9 eV for bare FTO and Pt SA/FTO, indicating that the electronic structure of the SnO_2 host is not measurably perturbed by the presence of Pt single atoms. The weak absorption tail observed below the band gap is commonly attributed to diffuse scattering and back-reflection effects arising from the textured FTO substrate, rather than to true sub-band-gap electronic states [48]. In contrast, the activity-matched PVD-Pt electrode exhibits a noticeably reduced transmittance across the visible spectrum and a modified sub-gap response, reflecting the intrinsic optical losses associated with thin metallic Pt films. This optical loss increases progressively with Pt loading, as shown by the transmittance spectra of the full PVD series (Figure S12). While the low-loading PVD electrodes (0.16–1.07 at%) still retain the transparency of bare FTO, they provide poor HER activity (Figure 3d,e) – namely when compared to the Pt_1^{2+}–O_4 system, and the loadings required for bulk-Pt-like kinetics (40–50 at%) result in substantial optical losses. That is, using conventional loading, a maximum in activity and transparency cannot be obtained at the same loading – single-atom electrode resolves this at a fixed, ultralow loading.

To directly assess the device-level implications of optical losses at the counter electrode, a sandwich-type photoelectrochemical cell was assembled using a Grätzel-type TiO_2/FTO photoanode and either Pt SA/FTO or an activity-matched PVD-Pt/FTO counter electrode. The TiO_2/FTO was prepared as in Ref. [49] (polycrystalline anatase, thickness ≈7 µm; details are given in Figure S13). Figure 6c,d show the corresponding *J*–*V* curves recorded in 0.1 M Na_2SO_4 under front-side illumination through the counter electrode using a 365 nm LED and a 325 nm laser source, respectively. For both excitation wavelengths, the photocurrent obtained with the Pt SA/FTO counter electrode is approximately 2–3 times higher than that achieved with the PVD-Pt electrode (Figure 6e).

When normalized to the Pt surface loading, the PEC-specific activity of the Pt SA/FTO counter electrode exceeds that of the PVD-Pt electrode by nearly four orders of magnitude (Figure 6f), underscoring the exceptional utilization efficiency of atomically dispersed Pt. Together, these results demonstrate that eliminating detrimental light absorption at the counter electrode—while maintaining bulk-like HER kinetics—directly provides superior photoelectrochemical performance, and highlights the remarkable advantage of optically invisible, highly active Pt single-atom catalysts for PEC device applications.

3 | Conclusions

In conclusion, we demonstrate that ultralow loadings of Pt (0.03 at%), stabilized as isolated single atoms (at a density of $\approx 3 \times 10^5$ SA µm^{-2}) by reactive deposition on fluorine-doped tin oxide (FTO), can deliver hydrogen-evolution reaction (HER) activities that approach those of bulk Pt while retaining full optical transparency across the UV–visible range. By exploiting the intrinsic conductivity and surface chemistry of FTO, Pt single atoms are anchored in an electronically coupled environment that enables efficient charge transfer without the need for metallic films or nanoparticle ensembles. As a result, HER performance comparable to conventional Pt electrodes is achieved at Pt loadings several orders of magnitude lower than those typically required for transparent counter electrodes and is retained over extended potential cycling. Experimental results are elucidated by theoretical calculations, which suggest that Pt SA is strongly anchored to the FTO surface and remains stable at both the solid|vacuum and solid|electrolyte interfaces under HER operating conditions, regardless of pH. Furthermore, the energetics of the H_{ads} on Pt SA/FTO are consistent with the observed high HER activity.

Electrochemical measurements across acidic, neutral, and alkaline electrolytes reveal high apparent turnover frequencies (>500 s^{-1} at moderate overpotentials) achieved at low site density. This emphasizes the exceptional utilization efficiency of Pt in this configuration, highlighting single-atom anchoring on conductive oxides as a viable strategy to decouple catalytic performance from precious-metal loading.

Beyond the specific Pt/FTO system studied here, these findings establish a pathway to transparent and resource-efficient electrocatalysts: conductive oxides can act not merely as inert current collectors but as active platforms for stabilizing and electronically wiring single-atom catalytic sites. This concept is relevant not only for photoelectrochemical devices and tandem solar fuel architectures, but also for other optoelectronic energy-conversion systems where optical transparency and minimal noble-metal usage are simultaneously required.

Author Contributions

Jochen Schmidt: formal analysis. **Igor A. Pašti**: formal analysis. **Jihyeon Kim**: writing – original draft, methodology, formal analysis, investigation. **Bidyut Bikash Sarmac**: formal analysis. **Xin Zhou**: formal analysis. **Ana S. Dobrota**: formal analysis. **Dmitry E. Doronkinb**: formal analysis. **Patrik Schmuki**: conceptualization, writing – review

and editing, project administration, supervision, funding acquisition. **Natalia V. Skorodumova**: formal analysis.

Acknowledgements

The authors would like to acknowledge DFG and the Operational Program Research, Development and Education (European Regional Development Fund, Project No. CZ.02.1.01/0.0/0.0/15_003/0000416 of the Ministry of Education, Youth and Sports of the Czech Republic) for financial support. P.S. would particularly like to acknowledge the support of the Czech Science Foundation projects GA CR-EXPRO, 23–08019X. The authors would like to acknowledge the support of the Center for Nanoanalysis and Electron Microscopy (CENEM, Friedrich-Alexander-Universität Erlangen-Nürnberg). We acknowledge DESY (Hamburg, Germany), a member of the Helmholtz Association HGF, for the provision of beamtime (proposal number of I-20250952 EC). We thank the P65 beamline stuff of PETRA III for their assistance. A.S.D. and I.A.P. acknowledge financial support from the Serbian Ministry of Science, Technological Development, and Innovations (contract no. 451-03-34/2026-03/200146) and the Serbian Academy of Sciences and Arts (project F-190). The computations and data handling were enabled by resources provided by the National Academic Infrastructure for Supercomputing in Sweden (NAISS) at the National Supercomputer Center (NSC) at Linköping University, partially funded by the Swedish Research Council through grant agreement No. NAISS 2025/5-713.

Open access funding enabled and organized by Projekt DEAL.

Conflicts of Interest

The authors declare no conflicts of interest.

Data Availability Statement

The data that support the findings of this study are available in the supplementary material of this article.

References

1. T. Kim, S. B. Roy, S. Moon, et al., "Highly Dispersed Pt Clusters on F-Doped Tin (IV) Oxide Aerogel Matrix: An Ultra-Robust Hybrid Catalyst for Enhanced Hydrogen Evolution," *ACS nano* 16 (2022): 1625–1638, https://doi.org/10.1021/acsnano.1c10504.

2. H. Wen, B. Weng, B. Wang, et al., "Advancements in Transparent Conductive Oxides for Photoelectrochemical Applications," *Nanomaterials* 14 (2024): 591, https://doi.org/10.3390/nano14070591.

3. A. Masao, S. Noda, F. Takasaki, K. Ito, and K. Sasaki, "Carbon-Free Pt Electrocatalysts Supported on SnO_2 for Polymer Electrolyte Fuel Cells," *Electrochemical and Solid-State Letters* 12 (2009): B119, https://doi.org/10.1149/1.3152325.

4. M. Batzill and U. Diebold, "The Surface and Materials Science of Tin Oxide," *Progress in surface science* 79 (2005): 47–154, https://doi.org/10.1016/j.progsurf.2005.09.002.

5. R. S. R. K. U. Rathnayakage, T. M. W. J. Bandara, K. Wijayaratne, G. R. A. Kumara, L. A. de Silva, and K. Tennakone, "Fluorine-Doped Tin Oxide Thin Films With High Surface Conductance and Low Transparency for Boosting Performance in Dye-Sensitized Solar Cell Applications," *ACS Applied Energy Materials* 6 (2023): 8336–8348, https://doi.org/10.1021/acsaem.3c00058.

6. I. K. O. Popoola, M. A. Gondal, J. M. AlGhamdi, and T. F. Qahtan, "Photofabrication of Highly Transparent Platinum Counter Electrodes at Ambient Temperature for Bifacial Dye Sensitized Solar Cells," *Scientific Reports* 8 (2018): 12864, https://doi.org/10.1038/s41598-018-31040-1.

7. S. Harsha, R. K. Sharma, M. Dierner, et al., "Dewetting of Pt Nanoparticles Boosts Electrocatalytic Hydrogen Evolution Due to Electronic Metal-Support Interaction," *Advanced Functional Materials* 34 (2024): 2403628, https://doi.org/10.1002/adfm.202403628.

8. K.-C. Huang, Y.-C. Wang, P.-Y. Chen, et al., "High Performance Dye-Sensitized Solar Cells Based on Platinum Nanoparticle/Multi-Wall Carbon Nanotube Counter Electrodes: The Role of Annealing," *Journal of Power Sources* 203 (2012): 274–281, https://doi.org/10.1016/j.jpowsour.2011.11.031.

9. T. Aaltonen, M. Ritala, T. Sajavaara, J. Keinonen, and M. Leskelä, "Atomic Layer Deposition of Platinum Thin Films," *Chemistry of Materials* 15 (2003): 1924–1928, https://doi.org/10.1021/cm021333t.

10. X. Yin, Z. Xue, and B. Liu, "Electrophoretic Deposition of Pt Nanoparticles on Plastic Substrates as Counter Electrode for Flexible Dye-Sensitized Solar Cells," *Journal of Power Sources* 196 (2011): 2422–2426, https://doi.org/10.1016/j.jpowsour.2010.09.047.

11. Y.-S. Ko and Y.-U. Kwon, "Electrochemical Deposition of Platinum on Fluorine-Doped Tin Oxide: The Nucleation Mechanisms," *Electrochimica Acta* 55 (2010): 7276–7281, https://doi.org/10.1016/j.electacta.2010.07.009.

12. L. Matoh, I. K. Škofic, M. Čeh, and N. Bukovec, "A Novel Method for Preparation of a Platinum Catalyst at Low Temperatures," *Journal of Materials Chemistry A* 1 (2013): 1065–1069, https://doi.org/10.1039/C2TA00072E.

13. H.-Y. Chen, J.-Y. Liao, B.-X. Lei, D.-B. Kuang, Y. Fang, and C.-Y. Su, "Highly Catalytic Carbon Nanotube/Pt Nanohybrid-Based Transparent Counter Electrode for Efficient Dye-Sensitized Solar Cells," *Chemistry–An Asian Journal* 7 (2012): 1795–1802.

14. R. S. Moraes, E. Saito, D. M. G. Leite, M. Massi, A. S. da, and S. Sobrinho, "Optical, Electrical and Electrochemical Evaluation of Sputtered Platinum Counter Electrodes for Dye Sensitized Solar Cells," *Applied Surface Science* 364 (2016): 229–234, https://doi.org/10.1016/j.apsusc.2015.12.114.

15. P. Hu, Z. Huang, Z. Amghouz, et al., "Electronic Metal–Support Interactions in Single-Atom Catalysts," *Angewandte Chemie International Edition* 53 (2014): 3418–3421, https://doi.org/10.1002/anie.201309248.

16. S.-M. Wu and P. Schmuki, "Single Atom Cocatalysts in Photocatalysis," *Advanced Materials* 37 (2024): 2414889, https://doi.org/10.1002/adma.202414889.

17. X. Zhou, Y. Wang, N. Denisov, et al., "Pt Single Atoms Loaded on Thin-Layer TiO_2 Electrodes: Electrochemical and Photocatalytic Features," *Small* 20 (2024): 2404064, https://doi.org/10.1002/smll.202404064.

18. S. Qin, J. Will, H. Kim, et al., "Single Atoms in Photocatalysis: Low Loading is Good Enough!," *ACS Energy Letters* 8 (2023): 1209–1214, https://doi.org/10.1021/acsenergylett.2c02801.

19. Y. Lai, Z. Zhang, Z. Zhang, et al., "Electronic Modulation of Pt Nanoclusters Through Tuning the Interface of Pt-SnO_2 Clusters for Enhanced Hydrogen Evolution Catalysis," *Chemical Engineering Journal* 435 (2022): 135102, https://doi.org/10.1016/j.cej.2022.135102.

20. M. Hübner, D. Koziej, M. Bauer, et al., "The Structure and Behavior of Platinum in SnO_2-Based Sensors Under Working Conditions," *Angewandte Chemie International Edition* 50 (2011): 2841–2844.

21. Y. Wang, N. Denisov, S. Qin, et al., "Stable and Highly Active Single Atom Configurations for Photocatalytic H_2 Generation," *Advanced Materials* 36 (2024): 2400626, https://doi.org/10.1002/adma.202400626.

22. Y. Wang, S. Qin, N. Denisov, et al., "Reactive Deposition Versus Strong Electrostatic Adsorption (SEA): A Key to Highly Active Single Atom Co-Catalysts in Photocatalytic H_2 Generation," *Advanced Materials* 35 (2023): 2211814, https://doi.org/10.1002/adma.202211814.

23. X. Chen, B. Zhou, S. Yang, et al., "In Situ Construction of an SnO_2/G-C_3N_4 Heterojunction for Enhanced Visible-Light Photocatalytic Activity," *RSC Advances* 5 (2015): 68953–68963, https://doi.org/10.1039/C5RA11801H.

24. J. Li, C. Chen, J. Li, S. Li, and C. Dong, "Synthesis of Tin-Glycerate and It Conversion Into SnO_2 Spheres for Highly Sensitive Low-ppm-level Acetone Detection," *Journal of Materials Science: Materials in Electronics* 31 (2020): 16539–16547.

25. I. Đurasović, R. Peter, G. Dražić, et al., "Catalytically Active Oxidized PtO_x Species on SnO_2 Supports Synthesized via Anion Exchange Reaction for 4-Nitrophenol Reduction," *Nanomaterials* 15 (2025): 1159.

26. R. Zhang, X. Wang, S. Yu, et al., "Ternary $NiCo_2P_x$ Nanowires as pH-Universal Electrocatalysts for Highly Efficient Hydrogen Evolution Reaction," *Advanced Materials* 29 (2017): 1605502, https://doi.org/10.1002/adma.201605502.

27. Q. Yang, H. Liu, P. Yuan, et al., "Single Carbon Vacancy Traps Atomic Platinum for Hydrogen Evolution Catalysis," *Journal of the American Chemical Society* 144 (2022): 2171–2178, https://doi.org/10.1021/jacs.1c10814.

28. C. Tsounis, B. Subhash, P. V. Kumar, et al., "Pt Single Atom Electrocatalysts at Graphene Edges for Efficient Alkaline Hydrogen Evolution," *Advanced Functional Materials* 32 (2022): 2203067, https://doi.org/10.1002/adfm.202203067.

29. R. Zhang, Y. Li, X. Zhou, et al., "Single-Atomic Platinum on Fullerene C_{60} Surfaces for Accelerated Alkaline Hydrogen Evolution," *Nature Communications* 14 (2023): 2460, https://doi.org/10.1038/s41467-023-38126-z.

30. M. Li, J. Zheng, F. Zheng, et al., "Regulating Volmer–Tafel Kinetics in NiPt 1% Alloy by Oxyphilic Y-Doped NiO for Enhancing Large-Current Hydrogen Evolution," *ACS Applied Materials & Interfaces* 17 (2025): 49620–49629, https://doi.org/10.1021/acsami.5c12377.

31. G. Gao, G. Zhu, X. Chen, Z. Sun, and A. Cabot, "Optimizing Pt-Based Alloy Electrocatalysts for Improved Hydrogen Evolution Performance in Alkaline Electrolytes: A Comprehensive Review," *ACS Nano* 17 (2023): 20804–20824, https://doi.org/10.1021/acsnano.3c05810.

32. X. He, X. Han, X. Zhou, et al., "Electronic Modulation With Pt-Incorporated NiFe Layered Double Hydroxide for Ultrastable Overall Water Splitting at 1000 mA cm^{-2}," *Applied Catalysis B: Environmental* 331 (2023): 122683, https://doi.org/10.1016/j.apcatb.2023.122683.

33. X. Zhou, J. Kim, H. Kim, S. Zahra, and P. Schmuki, "Pt Single Atom Deposition by Direct Current Sputtering in the Gas-Scattering Regime—A Simple Approach to Controlled Single Atom Loading," *Chemsuschem* 18 (2025): 202500489, https://doi.org/10.1002/cssc.202500489.

34. D. Liu, X. Li, S. Chen, et al., "Atomically Dispersed Platinum Supported on Curved Carbon Supports for Efficient Electrocatalytic Hydrogen Evolution," *Nature Energy* 4 (2019): 512–518, https://doi.org/10.1038/s41560-019-0402-6.

35. Q. Cheng, C. Hu, G. Wang, Z. Zou, H. Ynag, and L. Dai, "Carbon-Defect-Driven Electroless Deposition of Pt Atomic Clusters for Highly Efficient Hydrogen Evolution," *Journal of the American Chemical Society* 142 (2020): 5594–5601, https://doi.org/10.1021/jacs.9b11524.

36. P. Kuang, Y. Wang, B. Zhu, et al., "Pt Single Atoms Supported on N-Doped Mesoporous Hollow Carbon Spheres With Enhanced Electrocatalytic H_2-Evolution Activity," *Advanced Materials* 33 (2021): 2008599.

37. Y. Shi, Z.-R. Ma, Y.-Y. Xiao, et al., "Electronic Metal–Support Interaction Modulates Single-Atom Platinum Catalysis for Hydrogen Evolution Reaction," *Nature Communications* 12 (2021): 3021, https://doi.org/10.1038/s41467-021-23306-6.

38. X. Cheng, Y. Lu, L. Zheng, et al., "Engineering Local Coordination Environment of Atomically Dispersed Platinum Catalyst via Lattice Distortion of Support for Efficient Hydrogen Evolution Reaction," *Materials Today Energy* 20 (2021): 100653, https://doi.org/10.1016/j.mtener.2021.100653.

39. J. Park, S. Lee, H.-E. Kim, et al., "Investigation of the Support Effect in Atomically Dispersed Pt on WO_{3-x} for Utilization of Pt in the Hydrogen Evolution Reaction," *Angewandte Chemie International Edition* 58 (2019): 16038–16042, https://doi.org/10.1002/anie.201908122.

40. X.-P. Yin, H.-J. Wang, S.-F. Tang, et al., "Engineering the Coordination Environment of Single-Atom Platinum Anchored on Graphdiyne for Optimizing Electrocatalytic Hydrogen Evolution," *Angewandte Chemie International Edition* 57 (2018): 9382–9386, https://doi.org/10.1002/anie.201804817.

41. H. Tian, X. Cui, L. Zeng, L. Su, Y. Song, and J. Shi, "Oxygen Vacancy-Assisted Hydrogen Evolution Reaction of the Pt/WO_3 Electrocatalyst," *Journal of Materials Chemistry A* 7 (2019): 6285–6293, https://doi.org/10.1039/C8TA12219A.

42. J. Zhang, Y. Zhao, X. Guo, et al., "Single Platinum Atoms Immobilized on an MXene as an Efficient Catalyst for the Hydrogen Evolution Reaction," *Nature Catalysis* 1 (2018): 985–992, https://doi.org/10.1038/s41929-018-0195-1.

43. J. N. Hansen, H. Prats, K. K. Toudahl, et al., "Is There Anything Better Than Pt for HER?," *ACS Energy Letters* 6 (2021): 1175–1180, https://doi.org/10.1021/acsenergylett.1c00246.

44. J. K. Nørskov, T. Bligaard, A. Logadottir, et al., "Trends in the Exchange Current for Hydrogen Evolution," *Journal of the Electrochemical Society* 152 (2005): J23–J26.

45. G. K. Gebremariam, A. Z. Jovanović, A. S. Dobrota, N. V. Skorodumova, and I. A. Pašti, "Hydrogen Evolution Volcano(es)—From Acidic to Neutral and Alkaline Solutions," *Catalysts* 12 (2022): 1541, https://doi.org/10.3390/catal12121541.

46. X. Li, W. Bi, L. Zhang, et al., "Single-Atom Pt as Co-Catalyst for Enhanced Photocatalytic H_2 Evolution," *Advanced Materials* 28 (2016): 2427–2431, https://doi.org/10.1002/adma.201505281.

47. Z. Tian, Y. Da, M. Wang, et al., "Selective Photoelectrochemical Oxidation of Glucose to Glucaric Acid by Single Atom Pt Decorated Defective TiO_2," *Nature Communications* 14 (2023): 142, https://doi.org/10.1038/s41467-023-35875-9.

48. S. B. Ameur, A. Barhoumi, H. Bel hadjltaief, et al., "Physical Investigations on Undoped and Fluorine Doped SnO_2 Nanofilms on Flexible Substrate Along With Wettability and Photocatalytic Activity Tests," *Materials Science in Semiconductor Processing* 61 (2017): 17–26, https://doi.org/10.1016/j.mssp.2016.12.019.

49. U. Kerketta, H. Kim, N. Denisov, and P. Schmuki, "Grätzel-Type TiO_2 Anatase Layers as Host for Pt Single Atoms: Highly Efficient and Stable Photocatalytic Hydrogen Production," *Advanced Energy Materials* 14 (2024): 2302998, https://doi.org/10.1002/aenm.202302998.

Supporting Information

Additional supporting information can be found online in the Supporting Information section.

Supporting File: aenm71493-sup-0001-SuppMat.docx.